Characterization of MAR-M247 Deposits Fabricated through Scanning Laser Epitaxy (SLE)

Amrita Basak[1] and Suman Das[2]
[1] George W. Woodruff School of Mechanical Engineering, Georgia Institute of Technology, 801 Ferst Drive, Atlanta, Georgia 30332-0405, USA

[2] George W. Woodruff School of Mechanical Engineering, Georgia Institute of Technology, 801 Ferst Drive, Atlanta, Georgia 30332-0405, USA & School of Materials Science and Engineering, Georgia Institute of Technology, 771 Ferst Drive NW, Atlanta, Georgia 30313, USA

Abstract

This paper aims to characterize the microhardness and the process-induced residual stress in nickel-base superalloy MAR-M247 fabricated using a laser-powder bed fusion (LPBF)-based additive manufacturing (AM) process, scanning laser epitaxy (SLE). The SLE fabricated MAR-M247 samples are investigated using optical microscopy, scanning electron microscopy, x-ray diffraction, and Vickers microhardness measurements. The results show that the average Vickers microhardness values do not show any significant variation with changes in SLE processing parameters. However, the microhardness values are unevenly distributed and show variations along the build direction and the laser movement direction. Overall the hardness values are within $\pm 2\sigma$ limits for all the SLE deposited MAR-M247 samples. The effect of heat treatment on the microhardness and the residual stress is also investigated. The results show that the microhardness increases and the residual stress decreases after the heat treatment. This work is sponsored by the Office of Naval Research through grant N00014-14-1-0658.

Keywords: Nickel-Base Superalloy, MAR-M247, Additive Manufacturing, Scanning Laser Epitaxy (SLE), Microstructure, Vickers Microhardness, Residual Stress

Introduction

Nickel-base superalloys are extensively used in the fabrication of the gas turbine hot-section components as they exhibit exceptional high-temperature strength, creep resistance and corrosion resistance. However, the hot-section components have a limited operating life due to material loss from abrasion, oxidation, and corrosion. Currently, these components are scrapped and replaced when the material loss exceeds certain limits. Hence, there is a great interest in developing an additive manufacturing (AM) technology that can restore the parent metallurgy at the damage locations for these parts. A detailed review on AM of nickel-base superalloys may be found elsewhere and is skipped here for brevity [1].

Scanning laser epitaxy (SLE) is a laser powder bed fusion (LPBF)-based AM process that creates polycrystalline or equiaxed (EQ), directionally solidified (DS), and single-crystal (SX) structures through the melting of superalloy powders onto similar chemistry superalloy substrates. The galvanometer-controlled movement of the high-power laser (0.2 to 2 m/s) and high-resolution raster scanning (20 to 200 μm line spacing) result in superior thermal control over the solidification process. SLE has previously been demonstrated to successfully deposit a number of popular hot-section superalloys such as IN100 [2], René 80 [3], MAR-M247 [4], René 142 [5], CMSX-4® [6-8], and René N5 [9, 10] on both similar and dissimilar chemistry substrates.

However, in SLE as the laser performs raster scans atop the powder bed, the samples are subjected to rapid heating and fast cooling resulting in an accumulation of residual thermal stresses in the samples. Characterization of the residual stress in the SLE fabricated parts is crucial, as the residual stress has critical influence on the mechanical properties [11]. Both destructive and non-destructive characterization techniques are available to measure residual stresses. The most commonly used non-destructive methods are X-ray and neutron diffraction, which are capable of providing near-surface and volumetric residual stress measurements in crystalline materials, respectively. However, these methods are complicated, expensive or time consuming and has drawbacks with regards to textured samples. Destructive methods include hole drilling, sectioning or contouring, and crack compliance or slitting. While destructive methods are capable of providing location-specific residual stress information, they also require the use of additional analysis to determine residual stresses from deformation behaviour [11].

MAR-M247 is a nickel-base superalloy that was developed in the 1970s [4]. The alloy demonstrates high creep strength, good castability, and excellent oxidation and corrosion resistance at elevated temperatures. The alloy contains a high volume fraction (62 vol. %) of secondary phase precipitates [Ni_3 (Al, Ti)] and a significant amount (13.7 wt. %) of refractory elements such as tantalum (Ta), tungsten (W), and molybdenum (Mo). MAR-M247 is extremely difficult to weld, and to date, limited literature is available on AM processing of MAR-M247 [9]. In the present work, multiple samples of MAR-M247 were produced by altering the processing parameters such as the laser power and the scan speed. These parameters were combined to define a new measure such as the scan energy density (E). The SLE processed samples were investigated using optical microscopy (OM), scanning electron microscopy (SEM), energy dispersive x-ray spectroscopy (EDS), and Vickers microhardness measurements. A previously developed MATLAB code was applied to extract necessary information from the digital images using quantitative metallography techniques [7]. Multiple Vickers hardness measurements were performed along the length and width of the samples. Residual stress measurements were also performed in the deposit region using x-ray diffraction (XRD). The SLE fabricated MAR-M247 samples were subjected to a commercially available heat treatment process and the residual stresses were evaluated for the heat-treated samples as well.

Experimental procedure, materials, and methods

A single-mode 1kW Ytterbium fiber laser (IPG Photonics, model: YLS-1000) was used in the present study. A 3-axis galvanometer scanning system (Cambridge Technology) was used to direct the laser on top of the powder bed and focus the laser beam to a spot size of 20 µm Gaussian beam radius. This ensured tight control of the energy density inside the melt pool. The SLE process was conducted inside a process chamber that was purged to less than 10 parts-per-million (PPM) oxygen at atmospheric pressure using 99.999% high-purity Argon. No preheating was done prior to the SLE processing and the substrate coupons as well as the pre-placed powder were initially at ambient temperature. The process was carried out on rectangular EQ cast MAR-M247 coupons having dimensions of 31.50 mm x 5.84 mm x 2.54 mm. Each substrate was placed into a 31.50 mm x 5.84 mm recession cut into an IN625 base-plate. Figs. 1(a) and 1(b) show an overview of equipment associated with the SLE process and the placement of substrate coupons and powder-bed, respectively. A raster scan was employed in the current study. The details about the experimental procedure can be found elsewhere and is skipped here for brevity [2].

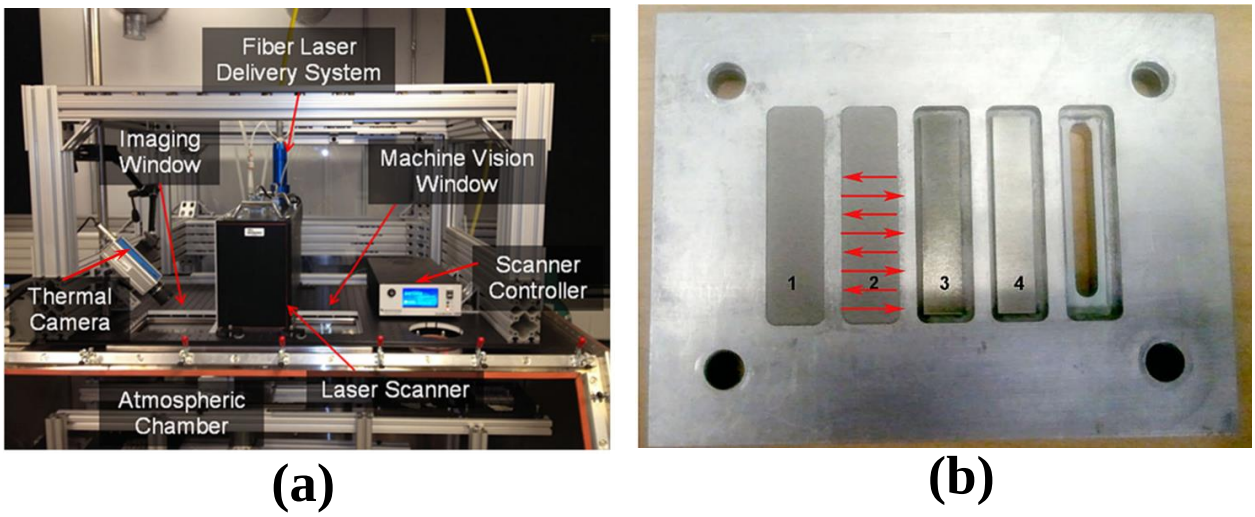

Figure 1. (a) The SLE workstation, (b) Placement of the superalloy coupons in the SLE process. The rightmost position shows the blank base to simulate the hollow passages below the tip in the high-pressure turbine blades. Positions 3 and 4 show the bare substrate coupons and positions 1 and 2 show the substrate coupons with pre-placed powder on top.

The MAR-M247 powder used in this study was an argon gas-atomized product made by Praxair Surface Technologies. The composition of the powder is reported in Table 1. The morphology, size distribution, and cross-sections of the powder were analysed using OM and SEM. The MAR-M247 powder particles were mostly spherical as shown in Fig. 2(a). The powder was mounted in Bakelite and polished to a mirror finish. The cross-section was analysed under an optical microscope for the inspection of internal porosity, and limited porosity was detected as shown in Fig. 2(b).

Table 1: Composition of the MAR-M247 powder (wt. %)

	Cr	Co	Mo	W	Al	Ti	Ta	Hf	B	C	Zr	Ni
MAR-M247	8.0	10.0	0.7	10.0	6.0	1.0	3.0	1.0	0.015	0.15	0.05	Bal

A Buehler automated saw was used to section the samples for microstructural investigation. The samples were mounted in Bakelite and polished to a mirror finish; starting with 80 grit paper and progressively increasing the size to 1200 grit. The samples were then polished using 5 µm and 3 µm diamond solutions. Finally, the samples were polished using a 0.5 µm colloidal alumina suspension. The polished samples were then etched using Marble's reagent (50 ml HCl, 50 ml H_2O, and 10.0 gm $CuSO_4$) to eliminate the γ' phases and reveal the microstructure. Imaging was then completed using a Leica DM6000 optical microscope at 100x, 500x, and 1000x magnifications. SEM investigations were carried out on a Hitachi SU8230 SEM. Microhardness measurements were carried out using a Buehler microhardness indenter with a fixed load at 2000 gf. The hardness values were obtained in Vickers microhardness scale.

In order to relieve the residual stresses and enable precipitation of the strengthening phases, the samples were heated and kept at 1080 ^{o}C for an hour. Thereafter, the samples were cooled at

5.6 ºC /minute or faster to a temperature below 870 ºC. Samples were then given a typical commercial low-temperature precipitation heat-treat cycle consisting of 12 hours at 870 ºC, followed by air cooling at minimum average cooling rate of 5.6 ºC / minute to 650 ºC to fully develop the strengthening phases.

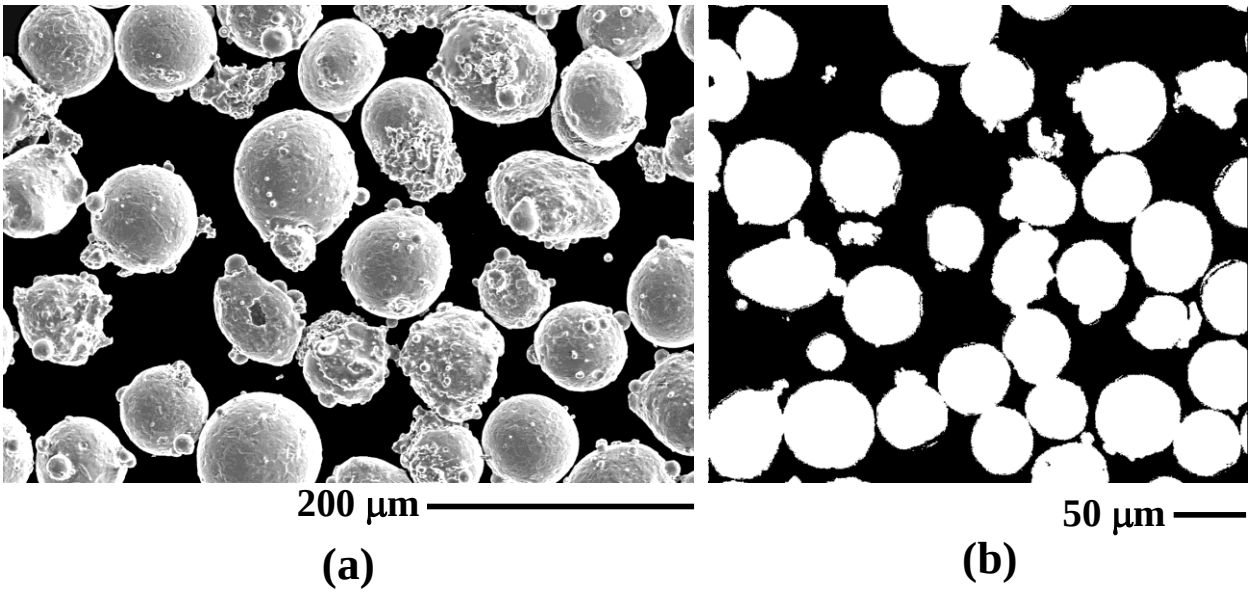

Figure 2. (a) SEM image of the MAR-M247 powder and (b) OM image of the powder cross-section.

Results and discussion

Deposit characteristics

Figs. 3(a) and 3(b) show two representative OM images of the SLE deposited MAR-M247 on EQ cast MAR-M247 substrates. These two samples were fabricated using E values of 26.51 J/mm^3 and 26.84 J/mm^3, respectively. Fig. 3(c) shows the OM image of Sample 1 after heat treatment. The deposits were crack-free and dense. An excellent metallurgical bond formed between the substrate and the deposit region, as shown in Figs. 3(a) and 3(b). The deposit region also shows a finer microstructure compared to the substrate region. The microstructural refinement may be attributed to the localized heating and rapid cooling due to the fast moving laser heat source. For all samples, SLE is demonstrated to deposit more than 1500 μm of average deposit height in a single pass.

The laser power (P) and the scan speed (V_S) were varied in the present study. All samples were run with a scan spacing (SS) of 25.4 μm to account for the smaller beam diameter of the fiber laser. The powder layer thickness (t_p) was kept as 1650 mm. A new measure was defined based upon the SLE processing parameters – the scan energy density, $E = \frac{\mathrm{P}}{\mathrm{SS} \times V_S \times t_P}$. Fig. 4(a) illustrates a representative microstructure of the SLE deposited MAR-M247 showing columnar dendrites. The columnar dendrites grew in the [001] direction and changed its structure to polycrystalline near

the top surface. The statistical analysis on the PDAS of the columnar dendrites was investigated for each sample in the longitudinal sections. A representative measurement is shown in Fig. 4(a). For each sample, 20 measurements were performed and the average PDAS values were calculated. Fig. 4(b) shows the effect of *E* on the PDAS. For the SLE deposited MAR-M247, the PDAS increased with *E* following a power-law relationship as shown in Fig. 4(b). Fig. 4(c) shows the effect *E* on the average deposit height. With an increase in *E*, the melt pool extended laterally and transversely allowing more powder to fall inside the melt pool, and thereby, increasing the deposit height.

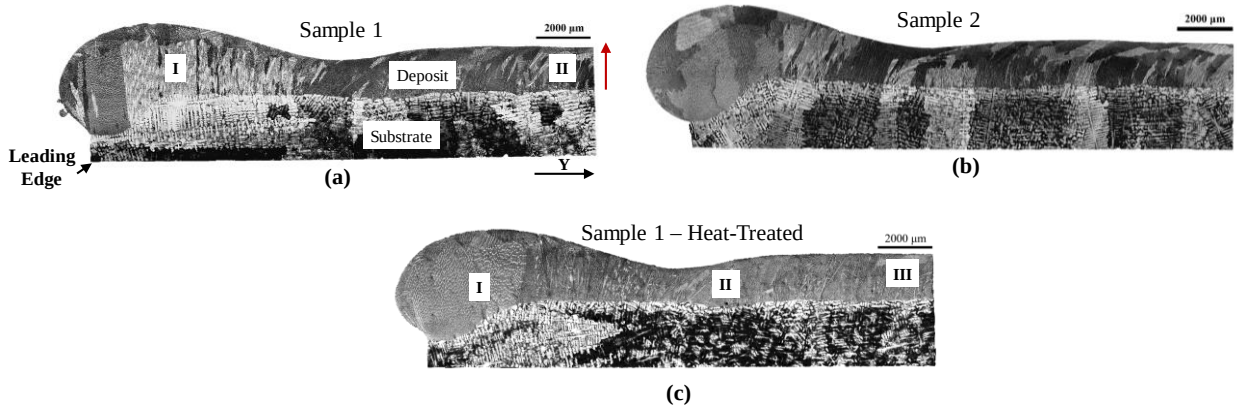

Figure 3. (a)-(b) Representative OM images of as-deposited MAR-M247 samples showing crack-free and dense deposit. The red arrow represents the build direction. (c) Representative OM image of a heat-treated MAR-M247 sample.

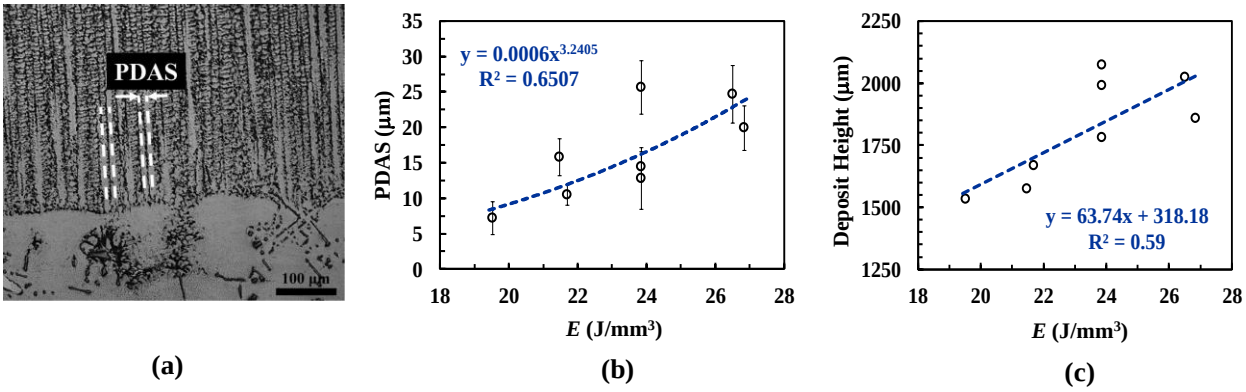

Figure 4. (a) OM image showing two representative measurement locations for PDAS. Effect of *E* on the (b) PDAS and (c) average deposit height.

Vickers microhardness

The average value of the cast substrate hardness ranges from 405 to 410 HV. The hardness increased significantly near the interface region showing values of order 430-440 HV. The deposit region showed hardness values ranging from 460-470 HV for the MAR-M247 sample. The deposit region showed hardness values in the range of 470-490 HV after the heat treatment. Increase in hardness values after the heat treatment is due to the homogenization of the microstructure [4].

However, variations in hardness value were observed in different regions of the deposit. The measurements were performed at 5 and 10 different locations along the Y direction and the X direction, respectively. Figs. 5(a) and 5(b) show the measurement grid points and two different representative indentation marks in the deposit region, respectively. The measurement pattern was chosen to accurately reflect the variation of hardness along the build direction and the laser movement direction. The average values of the hardness parameters were calculated as follows:

$$VH_{Average} = \left(\sum_{i=1}^{10} \sum_{j=1}^{5} VH \right) / 50 \tag{1}$$

$$\left(VH_X\right)_{i=1,2,3,\ldots,10} = \left(\left[\sum_{j=1}^{5} VH \right] / 5 \right)_{i=1,2,3,\ldots,10} \tag{2}$$

$$\left(VH_Y\right)_{j=1,2,3,\ldots,5} = \left(\left[\sum_{i=1}^{10} VH \right] / 10 \right)_{j=1,2,3,\ldots,5} \tag{3}$$

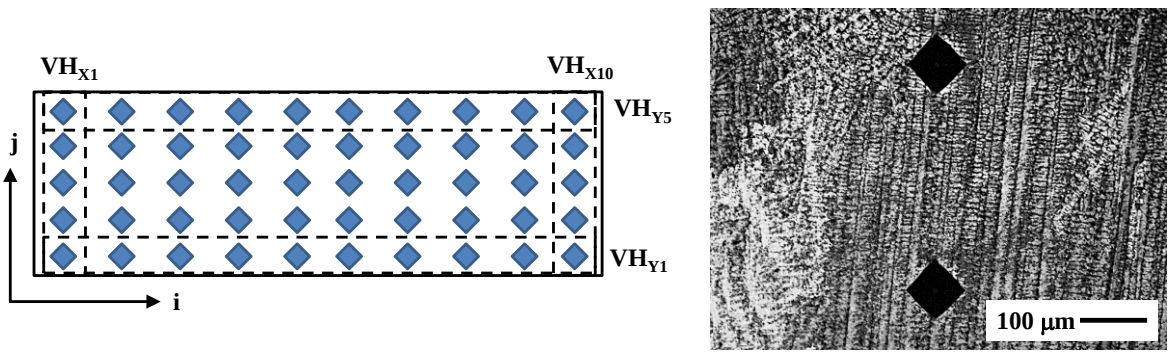

Figure 5. (a) Schematic of the measurement locations in the deposit and (b) representative indentation marks in the MAR-M247 deposit region.

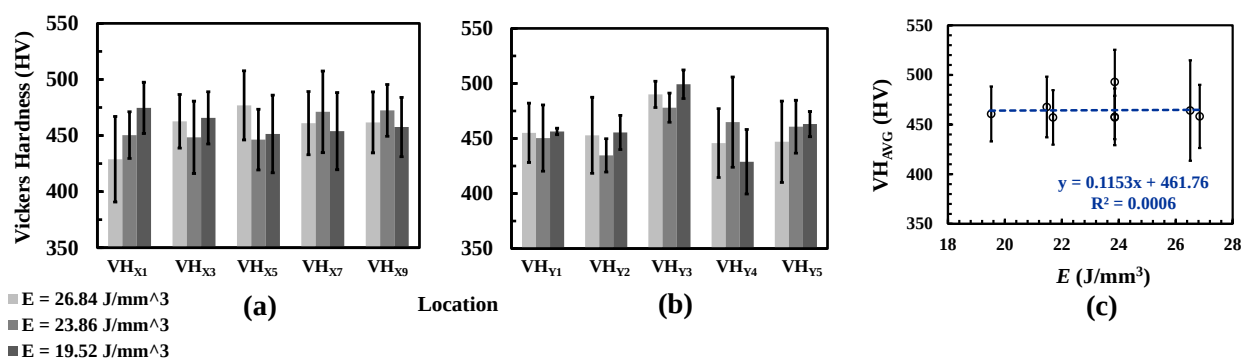

Figure 6. Variation of Vickers microhardness along the (a) build direction and (b) the laser movement direction for different values of *E* for as-deposited samples. (c) Effects of *E* on the average Vickers hardness in the deposit region for as-deposited samples.

The average value of the Vickers hardness was of the order of 460-490 HV for as-deposited samples and the variation was of order ±2σ along the build direction and the laser movement direction as shown in Figs. 6(a) and 6(b), respectively. With change in *E*, no significant changes were observed in the average hardness values as shown in Fig. 6(c). These results are encouraging as it signifies that changing the SLE processing parameters will have a minimal impact on the hardness distribution in the deposit region with most of the variation originating due to the variations in the local microstructure. In order to achieve uniform hardness values in the deposit region, the SLE process may be performed at lower *E*.

Residual stress measurements

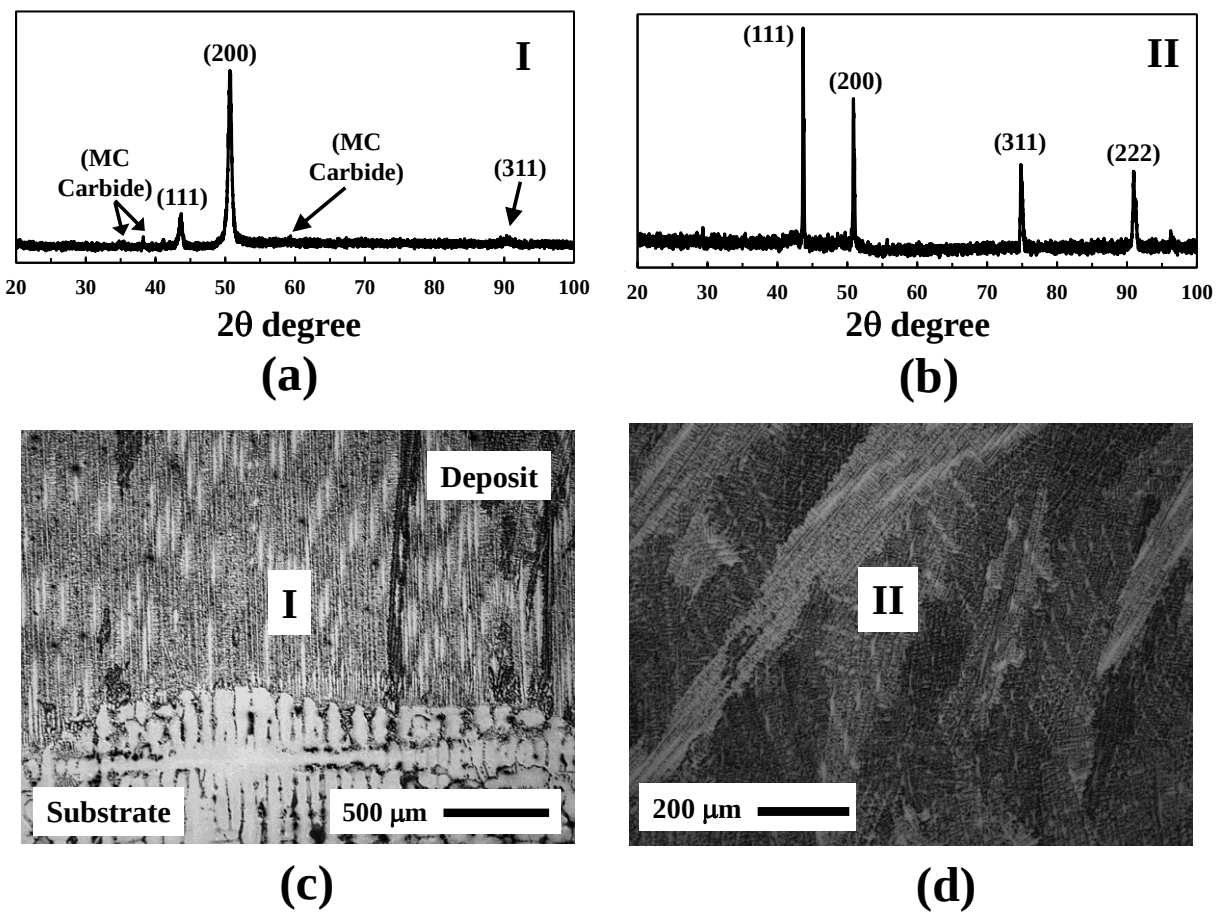

Figure 7. XRD profiles at (a) location I and (b) location II in Fig. 3(a). OM images showing MAR-M247 microstructure at (c) location I and (d) location II.

XRD measures lattice spacing based on Bragg's law: $\lambda=2d\sin\theta$. Here θ is the angle between the incident beam and the (hkl) lattice plane, d is the lattice spacing of the (hkl) plane of interest, and λ is the incident x-ray wavelength. It has been shown that there is a clear relationship between the diffraction pattern that is observed when X-rays are diffracted through crystal lattices and the distance between atomic planes (the inter-planar spacing) within the material. By altering the inter-

planar spacing different diffraction patterns will be obtained. The inter-planar spacing of a material that is free from strain will produce a characteristic diffraction pattern for that material. When a material is strained, elongations and contractions are produced within the crystal lattice, which change the inter-planar spacing of the (hkl) lattice planes.

This induced change in d will cause a shift in the diffraction pattern. By precise measurement of this shift, the change in the inter-planar spacing can be evaluated and thus the strain within the material deduced. The most commonly used method for stress determination is the $\sin^2\psi$ method. A number of XRD measurements are made at different ψ tilts. The inter-planar spacing, or 2θ peak position, is measured and plotted. The stress can then be calculated from such a plot by calculating the gradient of the line and with basic knowledge of the elastic properties of the material. This assumes a zero stress at $d = d_n$, where d is the intercept on the y-axis when $\sin^2\psi = 0$. More complex solutions exist for non-ideal situations where, for example, ψ splitting occurs (caused by the presence of shear stresses) or there is an inhomogeneous stress state within the material [12]. Details on the residual stress measurements using XRD may be found elsewhere, and, is skipped here for brevity [12].

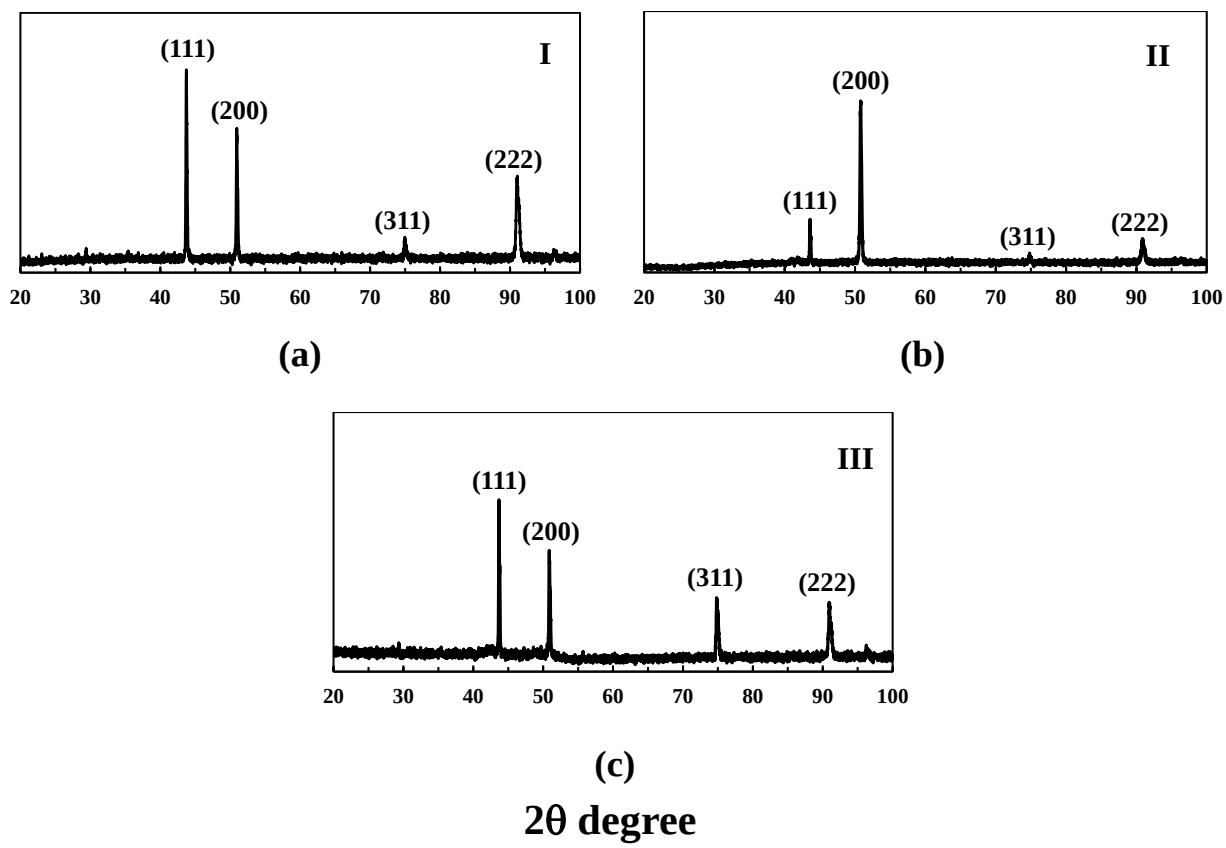

Figure 8. XRD profiles at (a) location I, (b) location II, and (c) location III in Fig. 3(c).

Fig. 7(a) shows the XRD profile at location I in Fig. 3(a) in the deposit region. A major peak at around 51° indicates a strong presence of γ solid solution and/or γ' phase in the SLE deposited MAR-M247. These two phases are typically difficult to differentiate because both γ and γ' phases

have cubic structures with less than 0.5% difference in lattice parameters for most commercial nickel-base superalloys [4]. The strong (200) peak at location I represents a unidirectional growth in the MAR-M247 deposit. Fig. 7(c) illustrates the OM image of location I showing a columnar growth in the deposit region. Fig. 7(b) shows the XRD profile at location II in Fig. 3(a). The strong peak at (200) was not present and the deposit region showed a prominent (111) peak. The OM image of location II is shown in Fig. 7(d). Figs. 7(a) and 7(b) also show a few minor peaks at 34°, 38°, and 58°. These peaks were due to the presence of MC (where M = metal) carbides. MAR-M247 contains about 0.05 wt. % C which resulted in the formation of carbide precipitates in the deposit region. Overall, different regions of the deposit showed different XRD peaks for MAR-M247 samples. Figs. 8(a) through 8(c) show the XRD profiles at locations I, II, and III in Fig. 3(c) in the deposit region showing the variation in crystal orientation in the deposit region of a representative heat-treated MAR-M247 sample.

The average stress was of order 257.5 ± 63.3 MPa for the as-deposited sample while 179.2 ± 33.3 MPa for the heat-treated sample. While heat treatments modify the microstructure and precipitation characteristics [4], such treatments were effective in relieving the residual stresses built within the SLE fabricated MAR-M247 deposit. The residual stresses in the deposit region for the heat-treated sample at locations I and III in Fig. 3(c) were 188 ± 26.2 MPa and 170.3 ± 40.4 MPa, respectively. The residual stress values were of similar order indicating that the heat-treatment was effective in homogenizing the stresses throughout the deposit region.

Conclusions

The difficulties associated with welding of high γ' nickel-base superalloys are well established. However, the current study showed excellent results for additive deposition of MAR-M247 using an LPBF-based AM approach. The processing conditions were varied and successful deposits were obtained across a broad range of operation parameters. The processing parameters were conveniently combined to define a new measure such as the scan energy density (E). The average deposit height was found to increase with E. However, no such relationship was observed for the average hardness values.

The hardness values showed variations of order $\pm 2\sigma$ along the build and the laser movement directions. The microstructures of MAR-M247 exhibited recrystallization after the heat-treatment. However, the microstructures became uniform after the heat treatment with approximately 31 % reduction in the residual stress. In the future, detailed investigations will be carried out to compare the experimentally measured residual stresses with finite element based simulations. The effect of heat treatment on the grain texture and distribution will also be analyzed using XRD.

Acknowledgements

This work was sponsored by the Office of Naval Research Cyber-Enabled Manufacturing Systems program through grant N00014-11-1-0670. The authors would like to thank the School of Materials Science and Engineering, Georgia Institute of Technology for providing machine time to perform the XRD experiments, Prof. Hamid Garmestani, School of Materials Science and Engineering, Georgia Institute of Technology for his valuable insight on analyzing the XRD data,

and Mr. David Tavakoli, PANalytical XRD facilities manager, Materials Characterization Facility, Georgia Institute of Technology for his assistance with performing the XRD experiments.

Disclosures

Dr. Suman Das is a co-founder of DDM Systems, a start-up company commercializing the SLE technology. Dr. Das and Georgia Tech are entitled to royalties derived from DDM Systems' sale of products related to the SLE research described in this paper. This study could affect their personal financial status. The terms of this arrangement have been reviewed and approved by Georgia Tech in accordance with its conflict of interest policies.

References

[1] Basak A, Das S. Epitaxy and Microstructure Evolution in Metal Additive Manufacturing. Annual Review of Materials Research 2016;46:125-49.

[2] Acharya R, Das S. Additive Manufacturing of IN100 Superalloy Through Scanning Laser Epitaxy for Turbine Engine Hot-Section Component Repair: Process Development, Modeling, Microstructural Characterization, and Process Control. Metallurgical and Materials Transactions A 2015:1-12.

[3] Acharya R, Bansal R, Gambone JJ, Kaplan MA, Fuchs GE, Rudawski N, et al. Additive Manufacturing and Characterization of René 80 Superalloy Processed Through Scanning Laser Epitaxy for Turbine Engine Hot‐Section Component Repair. Advanced Engineering Materials 2015;17:942-50.

[4] Basak A, Das S. Microstructure of nickel-base superalloy MAR-M247 additively manufactured through scanning laser epitaxy (SLE). Journal of Alloys and Compounds 2017;705:806-16.

[5] Basak A, Das S. A Study on the Microstructural Characterization of René 142 Deposited Atop René 125 Processed through Scanning Laser Epitaxy. Materials Science Forum 2016;879:187-92.

[6] Acharya R, Bansal R, Gambone JJ, Das S. A Coupled Thermal, Fluid Flow, and Solidification Model for the Processing of Single-Crystal Alloy CMSX-4 Through Scanning Laser Epitaxy for Turbine Engine Hot-Section Component Repair (Part I). Metallurgical and Materials Transactions B 2014;45:2247-61.

[7] Acharya R, Bansal R, Gambone JJ, Das S. A Microstructure Evolution Model for the Processing of Single-Crystal Alloy CMSX-4 Through Scanning Laser Epitaxy for Turbine Engine Hot-Section Component Repair (Part II). Metallurgical and Materials Transactions B 2014;45:2279-90.

[8] Basak A, Acharya R, Das S. Additive Manufacturing of Single-Crystal Superalloy CMSX-4 through Scanning Laser Epitaxy –Computational Modeling, Experimental Process Development, and Process Optimization. Metallurgical and Materials Transactions A 2016;47:3845-59.

[9] Basak A, Das S. A Study on the Effects of Substrate Crystallographic Orientation on Microstructural Characteristics of René N5 Processed through Scanning Laser Epitaxy: Proceedings of the 13th Intenational Symposium of Superalloys. Superalloys 2016:1041-9.

[10] Basak A, Das S. Additive Manufacturing of Nickel‐Base Superalloy René N5 through Scanning Laser Epitaxy (SLE)− Material Processing, Microstructures, and Microhardness Properties. Advanced Engineering Materials 2017;19:1600690.

[11] Wang Z, Denlinger E, Michaleris P, Stoica AD, Ma D, Beese AM. Residual stress mapping in Inconel 625 fabricated through additive manufacturing: Method for neutron diffraction measurements to validate thermomechanical model predictions. Materials & Design 2017;113:169-77.
[12] Fitzpatrick M, Fry A, Holdway P, Kandil F, Shackleton J, Suominen L. Determination of residual stresses by X-ray diffraction. 2005.